SAND2013-10478C

A Sophisticated Model to Predict Ash Inhibition during Combustion of Pulverized Char Particles

Yanqing Niu[1*], Christopher R. Shaddix[2]

[1] Key Laboratory of Thermo-Fluid Science and Engineering, Ministry of Education, Xi'an Jiaotong University, Xi'an 710049, China

[2]Combustion Research Facility, Sandia National Laboratories, Livermore, CA 94550, USA

Corresponding author:

Yanqing Niu, Key Laboratory of Thermo-Fluid Science and Engineering, Ministry of Education, Xi'an Jiaotong University, Xi'an 710049, China
Fax: +86-029-82668703
Email: yqniu85@mail.xjtu.edu.cn

Colloquium: Heterogeneous Combustion and Material Synthesis

Paper Length (Method 1)		**Words**
Main text		2997
Equations	(25+0)* 7.6*1+(1+0)*7.6*2	205
Nomenclature	(36+4)*7.6	304
References	(20+2)*2.3*7.6	385
Table 1	(9+2)*7.6*2	167
Figure 1	(40+10)*2.2*1+11	121
Figure 2	(35.5+10)*2.2*1+8	97
Figure 3	(90+10)*2.2*2+82	522
Figure 4	((49+10)*2)*2.2*1+46	305
Figure 5	(80+10) *2.2*2+13	409
Figure 6	((49+10)*2)*2.2*1+27	287
Total		**5799**

No color reprints necessary

Abstract

Final burnout of char particles from practical fuels such as coal and biomass occurs in the presence of a large ash component. Also, newly utilized coal resources, such as those from India, often contain much larger ash fractions than have traditionally been utilized. In the past, the inhibitory influence of ash on pulverized coal particle combustion has been most frequently modeled using an ash film model, though such films are rarely found when examining partially combusted particles. Conversely, some measurements have suggested that mineral components exposed on the surface of burning pulverized coal (pc) particles may diffuse back into the char matrix, the effect of which can be modeled as an ash dilution effect. To explore the implications of these different ash inhibition models on the temporal evolution of char combustion during burnout, we have developed a new computational model that considers the possibility of an ash film effect, an ash dilution effect, or some arbitrary combination of the two effects acting in tandem, which is the most realistic scenario. This new model predicts that restricted diffusion through the ash film has a significant impact on the char burnout rate throughout its lifetime, whereas char dilution only inhibits combustion significantly when most of the char has been consumed and the combustion mode shifts from predominantly external diffusion control to mixed diffusion control, with sensitivity to both external and internal diffusion resistance. The comparison of the model predictions with experimental results also confirms the previously suggested need to include gasification reaction steps when modeling coal char combustion.

Keywords: ash; char; coal; combustion; burnout

Nomenclature:

Symbols			
A	pre-exponent factor (g/s/cm^2/atmn); surface area (cm^2)	Nu	Nusselt number (take as 2)
		q	overall burning rate per unit surface of char core (g/cm^2/s)
d	diameter (cm)	P	pressure (atm)
D	diffusion coefficient (cm^2/s)	Q	heat transfer (W)
E	activation energy (kJ/mol)	R	ideal gas constant (8.314J/mol/K)
$FCO2$	fraction of CO_2	S_g	internal specific surface area (cm^2/g$_C$)
h	convective heat transfer coefficient (W/cm^2/K)	Sh	Sherwood number (taken as 2)
k_d	mass transfer coefficient (s/cm)	T	temperature (K)
k_s	reaction constant (g/s/cm^2/atmn)	X	fraction of ash forming an ash film
m	mass (g)	Y	ash content
M	molar mass (g/mol)	Z	mass loss ratio
N	carbon conversion ratio	$\triangle H$	reaction heat release (J/g)
Greek alphabet			
α	mode of burning parameter	τ	tortuosity
γ	Stefan flow factor	σ_c	constriction factor
ρ	mass density (g/cm^3)	δ	thickness of ash film
η	internal effectiveness factor	ψ	structure parameter
θ	porosity	σ	Stefan-Boltzmann constant (W/m^2/K^4)
Φ	Thiele modulus	ε	char emissivity (taken as 0.8)
v	stoichiometry number	λ	thermal conduction coefficient (W/cm/K)
Subscript			
0	initial	ex	external
a	ash	g	bBulk gas
a,f	porous ash	in	internal
af	ash film	int	intrinsic
a,n	nonporous ash	heat	kinetic reaction
app	apparent	max	maximum
c	carbon	s	surface
cc	char core	O_2	molecular oxygen
cs	char core surface	p	particle
eff	effective		
superscript			
n	reaction order		

1. Introduction

A number of different char burnout models have been constructed over the years for application to fluidized bed or pulverized coal combustors, and some of these have considered the influence of ash on this process [1-6]. Whereas ash effects are unlikely to be important during the early stages of combustion of low-ash fuels, they become increasingly important during char burnout and can be important throughout the combustion lifetime for higher ash fuels, such as some biomass fuels formed from residuals from biochemical processing or from certain high-ash coals, such as are common in India [3].

The existing models have all concentrated on using some form of an "ash film" model, whereby the ash that is liberated during the combustion of the carbonaceous matrix accumulates on the particle surface and acts to hinder combustion by acting as a diffusional barrier to the transport of oxygen to the encapsulated char core. This model of the influence of ash undoubtedly is a sensible approach when considering fluidized bed combustion, wherein the use of larger fuel particles and moderate conversion temperatures results in significant buildup of ash on the particle surface. However, for pulverized coal particle combustion, the high particle temperatures attained during active char combustion can soften or melt the ash and allow diffusion of liberated ash components back into the char matrix itself, as suggested by scanning electron microscopy (SEM) with energy-dispersive x-ray spectroscopy (EDX) measurements of inorganic concentrations in the char matrix adjacent to pore surfaces [7]. The result of this process on subsequent char combustion is best modeled as an "ash dilution" impact. Also, the ash that does stay on the particle surface tends to bead into distinct ash structures, as seen in Fig. 1, rather than build up a cohesive film. In fact, experimental investigation of the physical interaction of ash and residual char has found little evidence for the common existence of ash films encapsulating the char [7-13]. Indeed, the

mineral-rich content of coal fly ash particles that appear under optical illumination to be char-like (i.e. black or dark gray) [13], is consistent with an ash dilution concept to mineral evolution, as opposed to the ash film concept. In contrast to the prevalent models of ash film inhibition of char combustion in the literature, ash dilution of char combustion has only been formally modeled once [14], where it was demonstrated that this phenomenon can have a dramatic influence on the apparent reaction order when fitting *n*th-order Arrhenius reaction kinetics to experimental data.

During so-called Zone I char combustion, favored by low temperatures and smaller, less reactive char particles, oxygen penetrates throughout the entire particle and the char burning rate is controlled solely by the chemical reaction and the total surface area available for reaction. During Zone II combustion, which is generally more relevant for pulverized coal combustion conditions, char oxidation is active both in the interior pores of the particle and on the particle surface, with incomplete penetration of oxygen through the particle, such that the burning rate is limited by the combined effects of chemical reaction, available surface area, and oxygen diffusion from the bulk gas to the external char surface and through the porous char. Both for Zone I and Zone II combustion, the char structure, including the surface available for reaction, the porosity, and the presence of mineral or ash constituents within the particle, plays an important role in determining the char oxidation rate. For this reason, there has been a trend in the literature towards the use of intrinsic char kinetics models, which in theory can address these structural effects throughout the oxidation process. Consistent with this trend, we have implemented our ash effects model using a transient intrinsic kinetics approach which calculates char reactions throughout the porous particle.

The purpose of this paper is to report on the predictions of a new model of pulverized char particle burnout that treats ash inhibition through either ash film or ash dilution effects, or as some combination of the two. Specifically, the new model allows for allocation of the ash liberated at the

particle surface to (a) form an ash film, (b) diffuse back into the particle and participate as a dilution effect, or (c) act as a user-designated fraction of the two effects. In this way, the relative impact of the different modes of ash inhibition can be evaluated, and, by comparing to experimental data on char combustion and burnout, insight can be achieved into the actual nature of the ash inhibition process during pulverized coal char combustion. In the remainder of this paper, the modeling approach is first described in detail. Then, the ability of the integrated ash model to describe practical char combustion is demonstrated by comparisons between the numerical simulations and experiment measurements of both particle temperature, T_p, and carbon burnout over a range of burning rates. Finally, the model predictions are interrogated with respect to the influence of ash film versus ash dilution modes of char reaction inhibition, as well as the influence of the total ash content and particle size.

2. Model Description

Figure 2 gives a schematic illustration of the integrated ash model. An initial char particle with a diameter d_0 is divided into N equally spaced concentric shells, and during combustion the particle is idealized as consisting of an external ash film and an internal char core where ash and carbon are distributed uniformly. It is assumed that some fraction, X, of the ash components liberated during combustion of each burned shell is used to thicken the ash film, and the rest is assumed to penetrate and be uniformly distributed in the char core.

For simplification of description and treatment, the model is divided into four sub-models: an integrated ash sub-model, an intrinsic kinetics sub-model, a diffusion sub-model, and an energy balance sub-model. The reacting char particle is assumed to be spherical and to have uniform properties throughout. Any catalytic effect of the ash constituents is neglected and the ash constituents are assumed to not vaporize or be eliminated from the reacting particle via some other

mechanism.

2.1 Integrated ash sub-model

The ash sub-model is mainly used to calculate the evolution of ash film thickness, δ, and the ash content, $Y_{a,cc}$, in the char core after each shell of carbon is removed. As the char particle burns, a designated fraction X ($0 \leqslant X \leqslant 1$) of the ash products liberated at the surface of the particle is used to form an ash layer. Therefore, based on the ash mass balance, the ash film thickness, δ, can be expressed as Eq. (1).

$$2\delta = \left(\frac{X\rho_{cc}(d_{cc}^3 - d_{ccc}^3)Y_{a,cc} + 6m_{af,cc}/\pi}{\rho_{a,n}(1-\theta_{a,f})} + d_{ccc}^3\right)^{\frac{1}{3}} - d_{ccc} \qquad (1)$$

where $\rho_{a,n}$, the nonporous ash density, is assumed to be 2.65×10^3 kg/m^3 [4], and $\theta_{a,f}$, the ash porosity, is assumed to be 0.25, which is on the high end of the range of critical ash film porosities recommended by Hurt et al. [4].

The time-dependent ash content in the char core is calculated according to Eq. (2), where $m_{c,cc}$ and $m_{a,cc}$ represent the carbon mass and the ash mass in the char core, respectively. The ash mass in the char core is calculated by means of Eq. (3), whereas the carbon mass is calculated in the kinetic reaction sub-model described in section 2.2.

$$Y_{a,cc} = m_{a,cc}/(m_{a,cc} + m_{c,cc}) \qquad (2)$$

$$m_{a,cc} = (1-X)\rho_{cc}\frac{\pi}{6}(d_0^3 - d_{cc}^3)Y_{a0} + \rho_{cc}\frac{\pi}{6}d_{cc}^3 Y_{a0} \qquad (3)$$

2.2 Intrinsic kinetics sub-model

The presence of ash constituents within the char particle changes its porosity, pore size distribution, specific internal surface area, as well as the diffusion resistance of gaseous reactants and products through the char pores [10,14-16]. Considering the effect of ash and porosity in the char particle, the overall burning rate, q_{heat}, consisting of the combination of the internal and external burning rates of the char is given by Eq. (4):

$$q_{heat} = (1 - Y_{a,cc} - \theta_{c,cc} + \eta \rho_{c,cc} S_g d_{cc} / 6) q_{c,\mathrm{int}} \qquad (4)$$

where $\theta_{c,cc}$ is the porosity of carbon, η is the internal effectiveness factor, S_g is the specific internal surface area of carbon, and η is a dimensionless factor obtained through Eq. (5), in which Φ is a generalized Thiele modulus for spheres as shown in Eq. (6). According to reference [15] Eq. (5) and Eq. (6) yield accurate approximations of η for reaction order n varying from 0 to 1.

$$\eta = \frac{1}{\Phi}[\coth(3\Phi) - \frac{1}{3\Phi}] \qquad (5)$$

$$\Phi = \frac{d_{cc}}{6}[\frac{(n+1) k_s S_g \rho_{c,cc} (P_{cs} / RT)^{(n-1)}}{2 D_{eff}}]^{1/2} \qquad (6)$$

The effective diffusivity factor, D_{eff}, defined in Eq. (7) includes the effects of carbon and ash by volume proportion. D is the molecular diffusivity of reactants, σ_c is the constriction factor, and τ is the tortuosity, with τ/σ_c assumed to be 6.0 [4,5]. Eq. (8) gives the specific internal surface area, S_g, where S_{g0} and ψ take values of 247 m^2/g and 3.0, respectively [12].

$$D_{eff} = \frac{D\sigma_c}{\tau}(\theta_{a,f} V_{a,cc} / V_{cc} + \theta_c V_{c,cc} / V_{cc}) \qquad (7)$$

$$S_g = (\rho_0 / \rho_c) S_{g0} (1 - N)(1 - \psi \ln(1 - N))^{1/2} \qquad (8)$$

The carbon burning rate per unit external surface of char core, $q_{c,int}$, is calculated according to an Arrhenius expression, as follows:

$$q_{c,int} = A_{int} \exp(-E_{int} / RT_{cc}) P_{cc}^{n_{int}} \qquad (9)$$

$m_{c,cc}$ is calculated according to Eq. (10):

$$\frac{m_{c,cc}(d_{ccc} / d_{cc})^3 - m_{c,ccc}}{\eta \rho_{c,cc} S_g d_{cc} q_{c,int} / 6} = \frac{m_{c,cc} - m_{c,ccc}}{q_{heat}} \qquad (10)$$

2.3 Diffusion sub-model

In Zone Ⅱ, the char reaction is controlled by both chemical reaction and diffusion. Thus, the reactant concentration on the surface of the char core, P_{cs}, and the maximum diffusion rate through the ash film, q_{max}, need to be calculated. Considering the effects of Stefan flow and the ash film, q_{max}

and P_{cs} are calculated according to Eq. (11) and Eq. (12) [4], where k_d, the mass transfer coefficient, is calculated according to Eq. (13).

$$q_{max} = k_d P/\gamma \ln[1/(1-\gamma P_g / P)] \quad (11)$$

$$P_{O_2,cs} = P/\gamma + \left[P_g - P/\gamma \right] \exp(q\gamma / k_d P) \quad (12)$$

$$k_d = \frac{ShDd_p \theta_{a,f}^{2.5} M_c}{RT_m \nu (Sh\delta d_c + \theta_{a,f}^{2.5} d_c^2)} \quad (13)$$

2.4 Heating balance sub-model

The char core temperature, T_{cc}, and the particle temperature, T_p, are computed through Eqs. (14)-(19), which consider the radiation heat transfer, convection heat transfer, and conductive heat transfer. The heat released through char oxidation in the char core is transferred to the ash film through conduction, and then is transferred to the surroundings through convection and radiation. The thermal conductivity coefficient of the ash film, λ_a, in Eq. (19) is given by reference [17].

$$Q_{rxn} = Q_{cond} = Q_{conv} + Q_{rad,p} \quad (14)$$

$$Q_{rxn} = [q_{O2,\,rxn}(FCO_2 \Delta H_{CO_2} + (1-FCO_2)\Delta H_{CO}) + q_{H2O,\,rxn} \Delta H_{H2O}] A_{cc} \quad (15)$$

$$Q_{cond} = \pi d_p d_{cc} \lambda_a (T_{cc} - T_p)/\delta \quad (16)$$

$$Q_{conv} = h(T_p - T_g) A_p \quad (17)$$

$$Q_{rad,p} = \sigma \varepsilon (T_p^4 - T_w^4) A_p \quad (18)$$

$$\lambda_a = 0.0015 T_p^{1.1} \quad (19)$$

3. Results and discussion

3.1 Benchmark

Fig. 3 shows a comparison of particle burning temperatures and carbon conversion ratios acquired by experiment and model predictions with or without the steam gasification reaction. It can be seen from Fig. 3a that without the gasification reaction, the char particle combustion temperature

increases more rapidly with increasing ambient oxygen concentration than experimentally measured. This is consistent with the results found by Hecht et al. [19,20], wherein the endothermic effect of gasification reactions moderates the char combustion temperature, particularly for combustion in elevated oxygen contents. Meanwhile, the predicted carbon conversion rates all compare well to the experimental data. This result is also consistent with the expected minor influence of gasification reactions on the predicted char burning rate. Hecht et al. found that the overall effect of the combined steam and CO_2 gasification reactions is to increase the carbon conversion rate by only 10% in typical oxy-fuel combustion environments [20]. Overall, the predicted trends are fairly insensitive to the assumed intrinsic char kinetic reaction order. For subsequent calculations, an oxidation reaction order of 0.1 was used.

The right panel of Fig. 3 shows that when both the oxidation reaction and the steam gasification reaction are considered in the model, the predicted values are very close to the experimental measurements. The corresponding kinetic parameters and resultant standard deviation relative to the data are listed in Table 1 for various pre-exponential factors of the gasification reaction, from which it can been seen that when $A_{H2O,int}$ is 3.0 the predictions are more accurate than when using a higher value of 5 or when neglecting the steam gasification reaction ($A_{H2O,int}$ = 0). Therefore, this rate for the steam gasification reaction was used for the subsequent simulations.

3.2 Model Predictions

3.2.1 Influences of ash film and ash dilution

The effects of ash film and ash dilution on char burning are illustrated in Fig. 4. It can be seen that with an increasing fraction of the liberated ash forming an ash film (i.e. with increasing X), the char particle temperature decreases almost immediately during burnout, and the char burnout time increases. Thus, during low to moderate levels of burnout, the ash dilution effect has a much smaller

influence on char particle combustion than the formation of an external ash film. In fact, Cloke et al. [6] have previously noted that the ash film model led to a greater reduction in the char burning rate during the early burnout of pulverized coal relative to what was measured experimentally. Indeed, qualitative comparison of measured char particle temperatures during burnout (Fig. 3) with the modeled results under similar conditions shown in Fig. 4 suggests that the best agreement with the data will be for an assumed ash film fraction of approximately 0.5.

The influence of the ash film is further explored in Fig. 4 by the inclusion of computed results for the same values of ash film fraction as previously considered, but with the ash film porosity artificially set equal to 1, thereby eliminating the practical effect of lower diffusion through the ash film. In this case, the formation of an ash film is seen to yield an essentially identical char particle combustion rate relative to the case of full ash dilution up to the point of 80% burnout, after which the ash diluted particle burns very slowly while the particle that ignores all ash effects continues actively burning to full burnout. This comparison, together with that for the case of restricted diffusion through the ash film, shows that the primary inhibition mechanism of the ash film is via its restriction on diffusion of reactants to the particle surface (as opposed to a heat transfer effect associated with the ash film). The results also demonstrate that the ash dilution model has almost no influence on char burning rates up to approximately 80% burnout (at least for char particles with initial ash contents around 20%, as modeled here), and then has a large impact as burnout proceeds towards completion. This finding is consistent with the one previously reported ash dilution modeling result [14].

The increasing effect of ash dilution at the last stage may be attributed to the transformation from predominantly external diffusion control to mixed diffusion control, wherein reactions proceed throughout the whole char core, rather than near the char surface. At this point, the reduced

availability of carbon within the ash-diluted char core has a pronounced effect on the char burning rate.

Fig. 5 shows the morphologies of the char particle with different carbon conversion ratios. It can be seen from the simulation results that with increasing carbon conversion ratio *N*, the ash content in the char core increases and the ash film becomes thicker. When *N* is greater than 0.8, the ash film thickness is significant, and char combustion slows, due to the increasing diffusion transport resistance. Meanwhile, the increasing accumulation of ash particles in the char core reduces the diffusion of reactants and products within the particle, further lowering the burning rate. SEM imaging of collected char particles appears to be qualitatively consistent with the computed evolution in char morphology.

3.2.2 Influences of ash content and particle size

It can be seen from Fig. 6 that smaller particles (at least down to the 50 μm considered here) burn at a higher particle temperature and a higher carbon conversion rate. Meanwhile, the particles with a higher ash content burn at a lower particle temperature but at a higher carbon conversion rate in the initial stage. As burnout proceeds and ash inhibition effects increase, the carbon conversion rate decreases relative to ash-free particles and becomes particularly slow for larger particles (which have built up thicker ash films). Note that the details of the predicted char combustion temperatures and carbon burnout rates are specific to the assumed ash film factor, which is set to a low value of 0.16 in these simulations. The slightly enhanced char conversion rate that is seen for ash-containing particles at low extents of burnout in Fig. 6 results from the contribution of ash to the overall char volume, reducing the density of carbon within the char core. This effectively means that the particle is larger than it would otherwise be without ash and therefore has a greater diffusive flux of reactants to the char surface than it would otherwise have (increasing its burning rate). However, the greater

diameter also means the radiant heat loss is greater, reducing the particle temperature. These two seemingly contradictory trends have been previously seen [14]. As char burnout proceeds, the development of an external ash film overcomes the enhanced diffusive transport effect to the particle and reduces the net diffusive flux to the surface of the char core.

4. Conclusions

A new intrinsic kinetics model for the transient combustion of pulverized coal char particles has been developed that allows the interrogation of ash dilution as well as ash film inhibition of char burnout. The model kinetics have been calibrated against char particle temperature measurements for size-classified high-volatile bituminous coal char particles burning in environments with different oxygen content. This benchmarking of the model revealed the need to include a steam gasification reaction, together with char oxidation, in order to give good agreement with the measured data trends. Model results show that for low to intermediate levels of burnout, ash dilution has virtually no influence on the char combustion process, whereas the formation of an ash film almost immediately reduces the char burning rate. At high extents of burnout, both the ash film inhibition and ash dilution inhibition play a strong role, presumably due to the high concentration of ash within the particle and the increasingly strong role of internal particle diffusion on the char burning rate. Simulations as a function of initial char ash content show that the char combustion rate is actually slightly enhanced during early stages of burnout, presumably due to the lower effective carbon density when ash is included in the char matrix.

Acknowledgements

The present work was supported by the China Postdoctoral Science Foundation funded project (2013M532046), the National Nature Science Foundation of China (51376147) and the U.S.

Department of Energy (DOE) National Energy Technology Laboratory's Power Systems Advanced Research Program. The authors gratefully acknowledge the contributions of Ethan Hecht and Manfred Geier for their assistance with laboratory experiments and FORTRAN code writing. Sandia National Laboratories is a multiprogram laboratory managed and operated by Sandia Corporation, a wholly owned subsidiary of Lockheed Martin Corporation, for U.S. DOE's National Nuclear Security Administration under contract DE-AC04-94AL85000.

References

[1] C. Chen, T. Kojima, Fuel Processing Technology 47 (1996) 215-232.

[2] H. T. Zhang, J. H. Yan, M. J. Ni, K. F. Cen, Combustion Science and Technology 174 (2002) 55-73.

[3] S. Jayanti, K. Maheswaran, V. Saravanan, Applied Mathematical Modelling 31 (2007) 934-953.

[4] R. Hurt, J.-K. Sun, M. Lunden, Combust. Flame 113 (1998) 181-197.

[5] J.-K. Sun, R.H. Hurt, Proc. Combust. Inst. 28 (2000) 2205–2213.

[6] M. Cloke, T. Wu, R. Barranco, E. Lester, Fuel 82 (2003) 1989-2000.

[7] M.M. Lunden, N.Y.C. Yang, T.J. Headley, C.R. Shaddix, Proc. Combust. Inst. 27 (1998) 1695–1702.

[8] R.H. Hurt, K.A. Davis, Proc. Combust. Inst. 25 (1994) 561–568.

[9] R.H. Hurt, K.A. Davis, N.Y.C. Yang, D. Hardesty, "The Origin and Properties of Unburned Carbon from Pulverized-Coal Combustion," EPRI technical report, EPRI TR-105743, Nov. 1995.

[10] R.H. Hurt, K.A. Davis, Combust. Flame 116 (1999) 662-670.

[11] J.-K. Sun, R.H. Hurt, Proc. Combust. Inst. 28 (2000) 2205-2213.

[12] O. Senneca, Fuel 87 (2008) 1207-1216.

[13] I. Kuloats, R.H. Hurt, E.M. Suuberg, Fuel 83 (2004) 223-230.

[14] J.J. Murphy, C.R. Shaddix, Combust. Flame 157 (2010) 535-539.

[15] D.R. Froment, K.B. Bischoff, Chemical reactor analysis and design, John Wiley and Sons, New York, 1990, p. 162.

[16] R.E. Mitchell, L.Q. Ma, B. Kim, Combustion and Flame 151 (2007) 426-436.

[17] H. R. Rezaei; R. P. Gupta; G. W. Bryant; J. T. Hart; G. S. Liu; C. W. Bailey; T. F. Wall; S. Miyamae; K. Makino; Y. Endo, Fuel 79 (13) (2000) 1697-1710.

[18] J.J. Murphy, C.R. Shaddix, Combust. Flame 144 (2006) 710-729.

[19] E.S. Hecht, C.R. Shaddix, A. Molina, B.S. Haynes, Proc. Combust. Instit. 33 (2011) 1699-1706.

[20] E.S. Hecht, C.R. Shaddix, M. Geier, A. Molina, B.S. Haynes, Combust. Flame 159 (2012) 3437-3447.

Table:

Table 1 Optimized kinetic parameters and corresponding standard deviation σ[a]

Reaction	$C+(1+FCO_2)O_2 \rightarrow (1-FCO_2)CO+FCO_2CO_2$			$C+H_2O \rightarrow CO+H_2$			σ	
	$A_{O2,int}$	$E_{O2,int}$	$n_{O2,int}$	$A_{H2O,int}$	$E_{H2O,int}$	$n_{H2O,int}$	*T*p	*N*
Kinetic	8000	150	0.1	0	222	0.5	*127*	*0.041*
Parameters	8000	150	0.1	3	222	0.5	**33**	**0.039**
	8000	150	0.1	5	222	0.5	*35*	*0.044*

[a]For all conditions, the bulk CO_2 concentration is only 4 vol%, so the CO_2 gasification reaction is ignored in the prediction.

Figures:

Fig. 1 SEM of ash from a 600 MW pulverized coal furnace

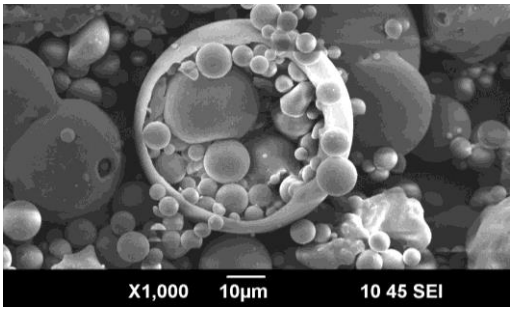

Fig. 2 Integrated ash film and ash dilution model

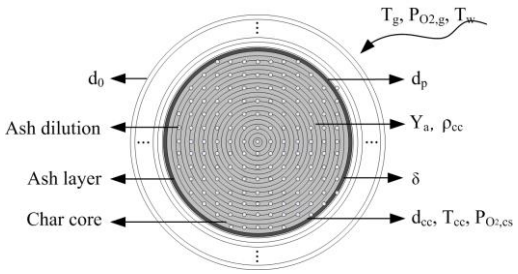

Fig. 3 Predicted and measured average temperatures and carbon conversion rate of a high volatile bituminous char particle for three different O_2 concentrations, 14 vol% moisture, and N_2 bath gas. The symbols show the measured data [18] and the lines show the model predictions. The panel on the right includes steam gasification, whereas that on the left does not. The initial char diameter is 115 μm, with an ash content of 26.3 wt%. The ash film factor is set to X = 0.16.

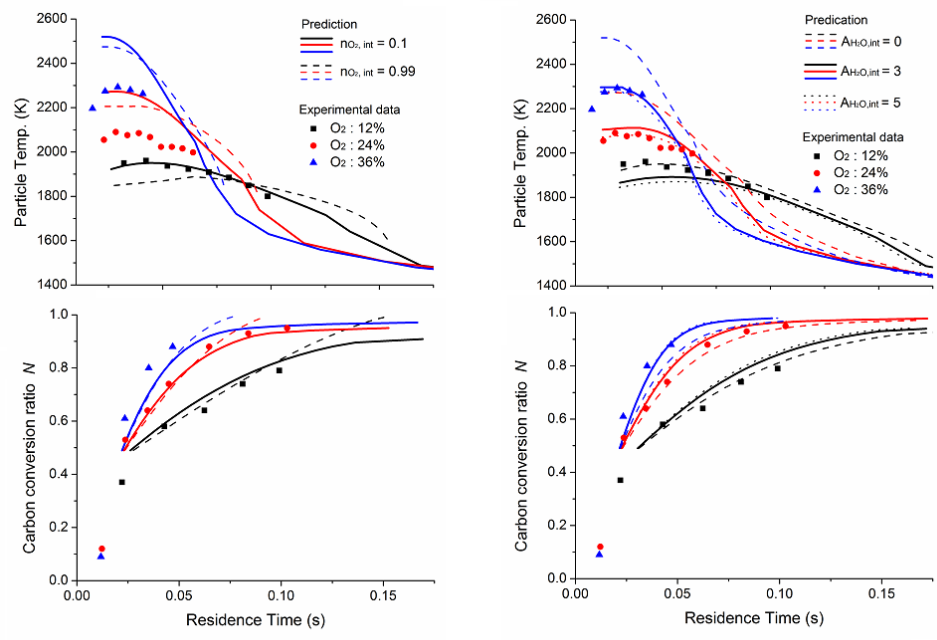

a. Single oxidation reaction

b. Oxidation reaction+Gasification reaction

Fig. 4 Effects of ash film and ash dilution on char burning. The initial char diameter is 100μm, its initial ash content is 20 wt%, and it is burning in a 1600 K environment with 24 vol% O_2, 14 vol% moisture, 58 vol% N_2 and 4 vol% CO_2.

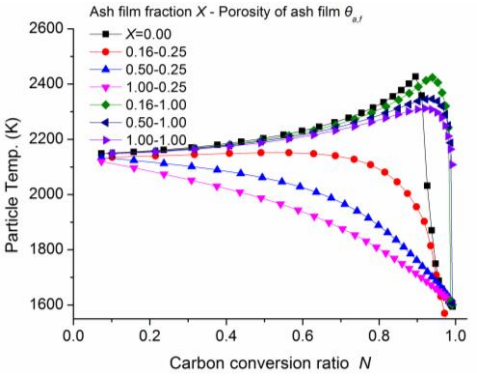

a. Particle temperature vs. carbon conversion ratio *N*

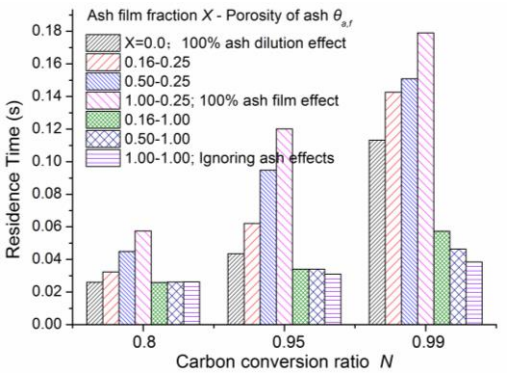

b. Residence time vs. *N*

Fig. 5 Ash evolution at different carbon conversion ratios *N*: experiment and simulation results

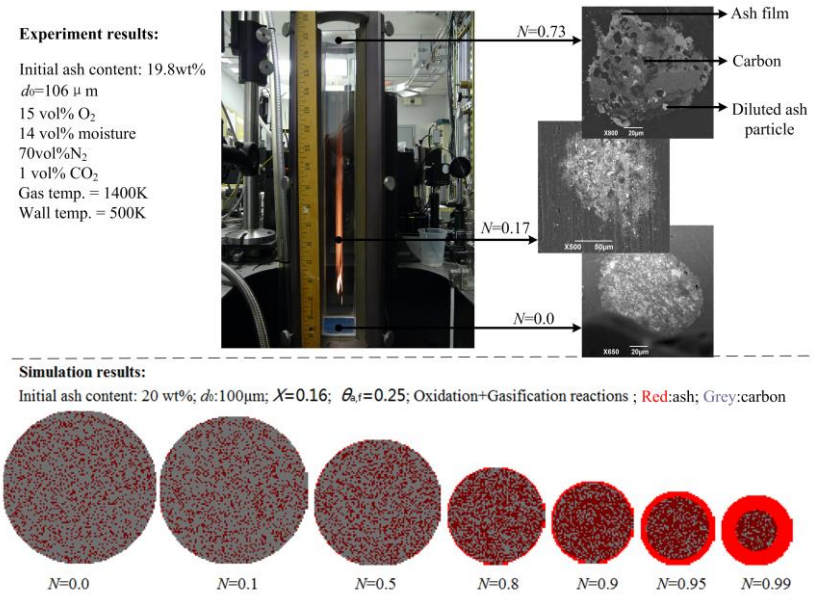

Fig. 6 Effects of initial ash content and particle size on char burning for the same conditions as Fig. 4, with an ash film factor X = 0.16.

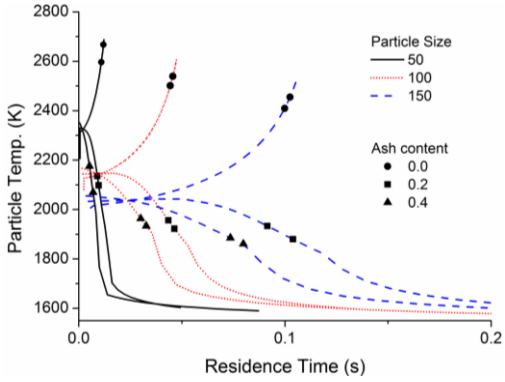

a. Particle temperature

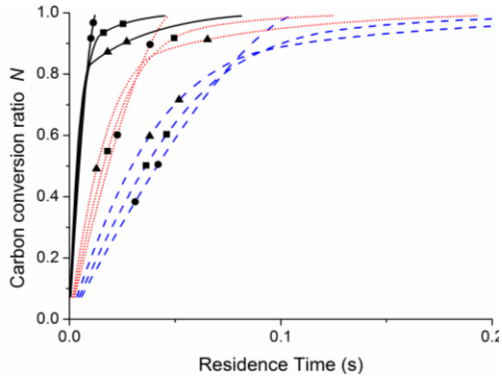

b. Carbon conversion ratio

Figure captions:

Fig. 1 SEM of ash from a 600 MW pulverized coal furnace

Fig. 2 Integrated ash film and ash dilution model

Fig. 3 Predicted and measured average temperatures and carbon conversion rate of a high volatile bituminous char particle for three different O_2 concentrations, 14 vol% moisture, and N_2 bath gas. The symbols show the measured data [18] and the lines show the model predictions. The panel on the right includes steam gasification, whereas that on the left does not. The initial char diameter is 115 μm, with an ash content of 26.3 wt%. The ash film factor is set to X = 0.16.

Fig. 4 Effects of ash film and ash dilution on char burning. The initial char diameter is 100μm, its initial ash content is 20 wt%, and it is burning in a 1600 K environment with 24 vol% O_2, 14 vol% moisture, 58 vol% N_2 and 4 vol% CO_2.

Fig. 5 Ash evolution at different carbon conversion ratios *N*: experiment and simulation results

Fig. 6 Effects of initial ash content and particle size on char burning for the same conditions as Fig. 4, with an ash film factor X = 0.16.